1,5-Disubstituted-1,2,3-triazoles as inhibitors of the mitochondrial Ca^{2+}-activated F_1F_O-ATP(hydrol)ase and the permeability transition pore.

Algieri V, Algieri C, Maiuolo L, De Nino A, Pagliarani A, Tallarida MA, Trombetti F, Nesci S. Ann N Y Acad Sci. 2021; 1485(1): 43-55.

The final published version is available online at:
https://doi.org/10.1111/nyas.14474

1,5-Disubstituted-1,2,3-triazoles as inhibitors of the mitochondrial Ca^{2+}-activated F_1F_O-ATP(hydrol)ase and of the permeability transition pore

Vincenzo Algieri[1a], Cristina Algieri[2a], Loredana Maiuolo[1]*, Antonio De Nino[1]*, Alessandra Pagliarani[2], Matteo Antonio Tallarida[1], Fabiana Trombetti[2], Salvatore Nesci[2]*

[1] Department of Chemistry and Chemical Technologies, University of Calabria, Via P. Bucci, cubo 12C, 87036 Rende (CS), Italy.

[2] Department of Veterinary Medical Sciences, University of Bologna, Ozzano Emilia Via Tolara di Sopra 50, Bologna, 40064, Italy.

[a] These authors contributed equally to this work

*Corresponding authors: Loredana Maiuolo loredana.maiuolo@unical.it; Antonio De Nino antonio.denino@unical.it; Salvatore Nesci salvatore.nesci@unibo.it

Abstract

The permeability transition pore (mPTP), an high-conductance channel triggered by a sudden Ca^{2+} concentration increase, involves the F_1F_O-ATPase. Since mPTP opening leads to mitochondrial dysfunctions, which feature many diseases, a great pharmacological challenge is to find mPTP modulators. In this study the effects of two 1,5-disubstituted 1,2,3-triazole derivatives, five-membered heterocycles with three nitrogen atoms in the ring and capable of forming secondary interactions with proteins, is investigated. Compounds **3a** and **3b** were selected among a wide range of structurally-related compounds, due to their chemical properties and their effectiveness in preliminary studies. In swine heart mitochondria both compounds inhibit the Ca^{2+}-activated F_1F_O-ATPase without affecting the F-ATPase activity sustained by the natural cofactor Mg^{2+}. The inhibition is mutually exclusive, probably because of their shared enzyme site, and uncompetitive with respect to the ATP substrate, since they only bind to the enzyme-ATP complex. Both compounds show the same inhibition constant (K'_i), but compound **3a** has a doubled inactivation rate constant compared to compound **3b**. Moreover, both compounds desensitize mPTP opening without altering mitochondrial respiration. The results strengthen the link between the Ca^{2+}-activated F_1F_O-ATPase and the mPTP and suggest that these inhibitors can be pharmacologically exploited to counteract mPTP-related diseases.

Keywords: triazole derivatives; mitochondria; F_1F_O-ATPase; permeability transition pore; calcium.

Short title: Triazole compounds effect on F_1F_O-ATPase and mPTP

1. Introduction

The mitochondrial permeability transition pore (mPTP) is a channel of the inner mitochondrial membrane (IMM), whose persistent formation induces abnormalities in the mitochondrial bioenergetic parameters (membrane depolarization, ion homeostasis loss, cessation of oxidative phosphorylation). [1] Lastly, mitochondrial swelling and rupture of the outer mitochondrial membrane cause different forms of cellular death. [2] Since the mPTP is increasingly involved in a variety of pathologies associated with mitochondrial dysfunctions, the molecular bioarchitecture that participates in mPTP formation represents a potential drug-target to counteract diseases featured by Ca^{2+} rise and cell death, including ischaemia-reperfusion injury, childhood neuromuscular diseases and age-related neurodegenerative diseases. [3] The mPTP was suggested to stem from the F_1F_O-ATPase(s), even if it is still controversial if the monomeric or the dimeric F_1F_O-ATPase form opens the pore. [4,5] The F_1F_O-ATPase is a bi-powered enzymatic engine that by means of the membrane embedded F_O domain uses the electrochemical gradient of H^+ obtained by mitochondrial respiration to synthetize ATP from ADP and Pi on hydrophilic F_1 domain. [6] The F_1F_O-ATPase can also work in reverse as H^+ pump and exploit the phosphoanhydride bond energy released by ATP hydrolysis to polarize the inner mitochondrial membrane [7]. The torque generation of the F_1F_O-ATPase rotor couples ATP synthesis/hydrolysis in the F_1 domain to H^+ translocation in the F_O domain. [8] However, this bi-functional activity, unique in nature, is only sustained by the natural cofactor Mg^{2+}, [9] while the substitution of Mg^{2+} by Ca^{2+} only allows the oligomycin-sensitive ATP hydrolysis, namely the coupling between F_1 and F_O. [10] The abrupt increase in matrix Ca^{2+} concentration associated with oxidative stress under physio-pathological conditions activates the F_1F_O-ATPase catalytic site, hydrolyzes CaATP and triggers mPTP formation. [11,12] These features make the Ca^{2+}-activated F_1F_O-ATPase an intriguing therapeutic target. [13] Any compound which inhibits the mPTP can address drug design and also provide new insights into the mPTP structure. Nowadays, the only accepted positive regulator of mPTP opening is the cyclophilin D (CyPD), a *cys-trans* peptidyl-prolyl isomerase in the mitochondrial matrix. [14] Cyclosporine A (CSA) and analogues which bind the CyPD are CyPD-dependent mPTP inhibitors, [3] which act by inhibiting CyPD and consequently mPTP. However, in CyPD knocked-out cells the CsA-mediated mPTP inhibition mechanism is abolished and the Ca^{2+} threshold required for mPTP opening is strongly increased. [14] Thus, CsA effect is limited by its target availability, which determines its efficacy. The failed clinical success of CsA and derivatives is also due to the physicochemical properties, *i.e.* poor hydrosolubility and high molecular weight, associated with cytotoxicity, undesired biological targets and poor blood-brain barrier permeability. [3,15]

The 1,2,3-Triazoles are a relevant class of five-membered N-heterocycles with intriguing biological activities, including antibacterial, anticancer and antivirus efficacy. [16] Their chemical structure with three vicinal nitrogen atoms in the ring and their aromatic nature make this class of compounds resistant to many reactions such as to oxidation, reduction and acid or basic hydrolysis. [17] Moreover, triazoles have the same capability of forming hydrogen bonds as well as dipole-dipole and π–staking interactions with various biological targets. These interactions can become even more relevant when several substituents are present on the backbone of these molecules. [18] For the synthesis of substituted 1,2,3-triazoles, the classical 1,3-dipolar cycloaddition of Huisgen between terminal alkynes and azides provides a mixture of 1,4- and 1,5-disubstituted triazoles. [19] This reaction was overcome from the introduction of copper or ruthenium salts as catalysts, obtaining the 1,4- or 1,5-regioisomer, respectively. [20,21] More recently, new synthetic procedures were realized by eliminative azide-olefin cycloaddition (EAOC) between substituted azides as dipole and electron deficient alkenes as dipolarophile, bypassing the problems that result from the use of only terminal alkynes. [22,23] In particular, nitroolefins received good deal of attention for their ability to furnish triazoline intermediates in high yields that readily decompose to triazoles, [24,25] while enaminones were a very good starting material to synthesized 1,4,5-trisubstituted triazoles, improving the properties deriving by multiple substituents on triazole ring. [26]

Recently, triazole derivatives, obtained by replacing the isoxazole core in analogue compounds, have been considered as second-generation inhibitors of the mPTP. Accordingly, this chemical modification was proven to improve plasma stability. [27] Indeed, drugs with a short half-life ($t_{½}$) in plasma risk to be degraded prior to be able to exert any biological effect. Thus, small molecules as substituted 1,2,3-triazoles represent interesting compounds to evaluate the structure-activity relationship focusing on the F_1F_O-ATPase activity, the major playmaker of mPTP event, and to clarify their effect on the mPTP by via CyPD-independent mechanism. Among a wide variety of structurally-related compound, compounds **3a** and **3b** were selected for their chemical properties, which make them prone to interact with proteins and produce biological effects, and for their promising effectiveness on the F_1F_O-ATPase activity shown in our preliminary studies. The aim is to establish if these compounds, by interacting with the F_1F_O-ATPase complex, are able to block mPTP formation and preserve the Mg^{2+}-activated F_1F_O-ATPase functionality, namely the ATP building capability, without exerting mitochondrial toxicity.

2. Materials and Methods

2.1. Chemicals and reagents

Fura-FF and oligomycin were purchased from Vinci-Biochem (Vinci, Italy). Na_2ATP was obtained from Sigma–Aldrich (Milan, Italy). All other chemicals were reagent grade and used without purification. Quartz double-distilled water was used for all reagent solutions, except when differently stated. Reactions were monitored by TLC using silica plates 60-F264 commercially available from Merck. ^1H and ^{13}C NMR spectra were recorded at 300 and 75 MHz, respectively, in $CDCl_3$ using tetramethylsilane (TMS) as the internal standard (Bruker (Billerica,MA,USA) ACP300MHz). Chemical shifts are given in parts per million and coupling constants in Hertz. LC-MS analyses were carried using an Agilent 6540 UHD Accurate—Mass Q-TOFLC-MS fitted with an electrospray ionization source (DualAJSESI) operating in positive ion mode. Chromatographic separation was achieved using a C18 RP analytical column (Poroshell 120, SB-C18,50×2.1mm,2.7mm) at 30°C with an elution gradient from 5% to 95% of B over 13 min, a being H_2O (0.1%FA) and B CH3CN (0.1%FA). Flow rate was 0.4mLmin^{-1}.

2.2. Synthesis of 1-methyl pyridinium trifluoromethanesulfonate ([mpy]OTf)

1-Methyl pyridinium trifluoromethanesulfonate ([mpy]OTf) was prepared by halide-free direct synthesis as reported in literature. [28–30]

*2.3. General procedure for the synthesis of 1,5-disubstituted-1,2,3-triazoles **3a** and **3b***

In a two-necked round bottom flask, equipped with bubble condenser and magnetic stir bar, [mpy]OTf (5 mL), $FeCl_3$ (20 mol %), (*E*)-nitrostyrene derivative (**1a-1b)** (1 eq) and phenylazide **2** (2 eq) were placed. The reaction was conducted at 100°C. The crude was extracted with dichloromethane (3×5mL) and the combined organic layer was evaporated under vacuum. The crude product was purified on a flash silica gel column by using hexane/ethyl acetate (9:1 v/v) to obtain the desired product. Complete characterization of products **3a** and **3b** is reported in Supplementary Materials.

1-benzyl-5-phenyl-1,2,3-triazole (**3a**). White solid (mp. 69.7-70.2°C), y=95%.

^{1}H-NMR ($CDCl_3$, 300 MHz): δ (ppm) 5.55 (s, 2H, CH_2), 7.03-7.13 (m, 2H, Ar), 7.22-7.32 (m, 5H, Ar), 7.37-7.46 (m, 3H, Ar), 7.75 (s, 1H, CH). ^{13}C-APT NMR ($CDCl_3$, 75 MHz): δ (ppm) 51.83, 126.95, 127.17, 128.16, 128.84, 128.91, 128.97, 129.52, 133.30, 135.53, 138.17. ESI(+)-MS: m/z [M + H] calcd for $C_{15}H_{14}N_3$ 236.1182, found: 236.0952

1-benzyl-5-(2-nitrophenyl)-1,2,3-triazole **(3b).** Pale Yellow solid (mp. 82.5-83.4°C), y=91%.

^{1}H-NMR ($CDCl_3$, 300 MHz): δ (ppm) 5.42 (s, 2H, CH_2), 6.90-6.97 (m, 2H, Ar), 7.00 (d, 1H, J=7.67Hz, Ar), 7.14-7.29 (m, 3H, Ar), 7.55 (t, 1H, J=7.50Hz, Ar), 7.60-7.64 (m, 1H, Ar), 7.66 (s, 1H, CH), 8.12 (d, 1H, J=8.15Hz, Ar). ^{13}C-APT NMR ($CDCl_3$, 75 MHz): δ (ppm) 52.76, 122.14, 124.83, 127.68, 128.34, 128.64, 130.96, 132.99, 133.02, 133.17, 133.84, 134.30, 148.45. ESI(+)-MS: m/z [M + H] calcd for $C_{15}H_{13}N_4O_2$ 281.1033, found: 281.1016.

2.4. Preparation of the mitochondrial fractions

Immediately after slaughter, hearts from adult swine (*Sus scrofa domesticus*) were collected at a local abattoir and transported to the lab within 2 h in ice buckets at 0–4°C. After removal of fat and blood clots as much as possible, approximately 30–40 g of heart tissue were rinsed in ice-cold washing Tris-HCl buffer (medium A) that consists of 0.25 M sucrose, 10 mM Tris(hydroxymethyl)-aminomethane (Tris), pH 7.4. The tissue was finely chopped into fine pieces with scissors, gently dried on blotting paper and weighted. Each preparation was made from one heart. The chopped tissue was homogenized in a buffer (medium B) consisting of 0.25 M sucrose, 10 mM Tris, 1.0 mM EDTA (free acid), 0.5 mg/mL BSA, pH 7.4 with HCl at a ratio of 10 mL medium B per 1 g of fresh tissue. After a preliminary gentle break up by Ultraturrax T25, the tissue was carefully homogenized by a motor-driven teflon pestle homogenizer (Braun Melsungen Type 853202) at 650 rpm with 3 up-and-down strokes. To obtain the mitochondrial fraction by stepwise centrifugation (Sorvall RC2-B, rotor SS34), the homogenate was centrifuged at 1,000 *g* for 5 min, thus yielding a supernatant and a pellet. The latter was re-homogenized under the same conditions of the first homogenization and re-centrifuged at 1,000 *g* for 5 min. The supernatants from these two centrifugations gathered and filtered through four cotton gauze layers, were centrifuged at 10,500 *g* for 10 min to yield the raw mitochondrial pellet that was resuspended in medium A and further centrifuged at 10,500 *g* for 10 min to obtain the final mitochondrial pellet. The latter was resuspended by gentle stirring using a Teflon Potter Elvejehm homogenizer in a small volume of medium A, thus obtaining a protein concentration of 30 mg/mL. [31] All steps were carried out at 0–4°C. The protein concentration was determined according to the colorimetric method of Bradford [32] by Bio-Rad Protein Assay kit II, using bovine serum albumin (BSA) as standard. The mitochondrial preparations were then stored in liquid nitrogen until the evaluation of F-ATPase activities.

2.5. Mitochondrial F-ATPase activity assays

Immediately after thawing, mitochondrial preparations were used to evaluate the F-ATPase activity. The ATP hydrolysis capability was assayed in a reaction medium (1 mL) containing 0.15 mg mitochondrial protein and 75 mM ethanolammine–HCl buffer pH 9.0, 6.0 mM Na_2ATP and 2.0 mM $MgCl_2$ for the Mg^{2+}-activated F_1F_O-ATPase assay, and in the same buffer at pH 8.8 plus 3.0 mM Na_2ATP and 2.0 mM $CaCl_2$ to evaluate the Ca^{2+}-activated F_1F_O-ATPase activity. After 5 min preincubation at 37°C, the reaction, carried out at the same temperature, was started by adding the substrate Na_2ATP and stopped after 5 min by adding 1 mL of ice-cold 15% (w/w) trichloroacetic acid aqueous solution. Once the reaction was blocked, vials were centrifuged for 15 min at 3,500 rpm (Eppendorf Centrifuge 5202). The concentration of inorganic phosphate (Pi) hydrolyzed by known amounts of mitochondrial protein in the supernatant, which indirectly detects the F-ATPase activity, was spectrophotometrically evaluated. [33] To this aim, 1.0 µL from a mother solution of 3.0 mg/mL oligomycin in dimethylsulfoxide (DMSO) was directly added to the reaction mixture before starting the reaction. The total ATPase activity was calculated by the Pi evaluation in control tubes run in parallel and

containing 1.0 µL DMSO per mL reaction system. Control tubes were alternated to the condition to be tested in each set of experiments. The dose of 3.0 mg/mL oligomycin, specific inhibitor of F-ATPase which selectively blocks the F_O subunit, which is currently used in F-ATPase assays, [34] ensured maximal F-ATPase inhibition. The F_1F_O-ATPase activity, routinely measured by subtracting, from the Pi hydrolyzed by total ATPase activity, the Pi hydrolyzed in the presence of oligomycin, [35] was expressed as µmol Pi·mg protein^{-1}·min^{-1} in all experiments.

2.6. Kinetic analyses

The inhibition mechanism of **3a** and **3b** triazole derivatives on the Ca^{2+}- or Mg^{2+}-activated F_1F_O-ATPases was explored by the graphical methods of Dixon and Cornish-Bowden plots, which complement one another. [36] To this aim, the 1/*v* (reciprocal of the enzyme activity) in Dixon plot or the S/*v* ratio in Cornish-Bowden plot were plotted as a function of **3a** or **3b** concentration. In all plots the enzyme specific activity was taken as the expression of *v*. To build these plots, different experimental sets were designed in which the F-ATPase activity was evaluated in the presence of increasing triazole derivative concentrations at two ATP concentrations, keeping the metal cofactor (Mg^{2+} or Ca^{2+}) concentration constant. The values of K'_i, which represent the dissociation constant of the ternary *ESI* complex, were calculated as the abscissa (changed to positive) of the intercept of the straight lines obtained in the Cornish-Bowden plots.

To obtain time-course plots the F-ATPase reaction was carried out in the presence of 1 mM **3a** or **3b** triazole derivative, previously solubilized in DMSO, (directly added with the ATP substrate) in the reaction system and stopped after different time intervals (1-5 min) by TCA. Enzyme activity data were then plotted as percentages of the residual F-ATPase activity in the presence of 1 mM triazole derivative (**3a** or **3b**) (θ) versus the incubation time of the same compound. In this plot 100% F-ATPase activity corresponded to the initial enzyme activity (θ_i), assuming that the compound under study is not bound to the enzyme. By fitting the data in a semilogarithmic plot, straight lines were obtained according to the equation:

$$log\ \theta = -\frac{k_{inact}}{2.3}t + log\ \theta_i$$

In these plots the slope of each straight line corresponds to $-k_{inact}/2.3$ (angular coefficient) and the *y*-axis intercept to log θ_i. Thus, the inactivation rate constant (k_{inact}) for each triazole derivative was calculated from the slope (k_{inact}= slope·2.3·60^{-1}) and expressed as s^{-1}. [37,38]

Kinetic studies on the mutual exclusion of different inhibitors on the same F-ATPase activity were carried out in order to cast light on the possible interaction on F_1F_O-ATPase between triazole derivative **3a** and **3b**. To build Dixon-like plots, in which the reciprocal of enzyme activity data (1/*v*) (*y* axis) were plotted versus the concentration of triazole **3b** (*x* axis) at a constant ATP substrate concentration and in the absence and in the presence of r one fixed concentrations of triazole **3a**. [34] According to the graphical method employed, [39] when the straight lines are parallel, namely they have the same slopes, the enzyme inhibition mirrors the binding of either **3a** or **3b** to the enzyme and the two compounds mutually exclude.

2.7. Mitochondrial respiration assay

Immediately after thawing, the mitochondrial fractions were used to evaluate the mitochondrial respiration. The experiments on freeze-thawed mitochondria primarily aimed at clarifying the effects of the selected triazole compounds effects on mitochondrial respiratory chain enzyme activities and on the F_1F_O-ATPase. The experimental conditions adopted ruled out any potential concomitant effect of changes in the transmembrane electrochemical gradient of H^+. To detect mitochondrial respiratory activities, the oxygen

consumption rates were polarographically evaluated by Clark-type electrode using a thermostated Oxytherm System (Hansatech Instruments) equipped with a 1 mL polarographic chamber. The reaction mixture (120 mM KCl, 10 mM Tris-HCl buffer pH 7.2), maintained under Peltier thermostatation at 37°C and continuous stirring, contained 0.25 mg mitochondrial protein. [35]

To evaluate the NADH-O_2 oxidase activity, the mitochondrial oxidation was run under saturating substrate conditions (75 µM NADH) after 2 min of stabilization of oxygen signal. Preliminary tests assessed that under these conditions O_2 consumption was suppressed by 2.5 µM rotenone, known inhibitor of Complex I. [40] The succinate-O_2 oxidase activity by Complex II was determined by the succinate oxidation in the presence of 2.5 µM rotenone. The reaction was started by the addition of 10 mM succinate after 2 min of stabilization of oxygen signal. Also in this case preliminary tests assessed that, under the conditions applied, succinate oxidation was suppressed by of 1 µg/mL antimycin A, selective inhibitor of complex III. [40]

To evaluate the effects of the compounds under study, the mitochondrial suspensions were added at the same time as the triazole **3a** or **3b** solutions of adequate concentrations, to the polarographic chamber before starting the reaction at 37°C. Triazole solutions of adequate concentrations were prepared immediately before the experiments by dissolving the compounds in DMSO. The mitochondrial respiratory rate was automatically evaluated by O_2view software and expressed as nmoles O_2·mg protein^{-1}·min^{-1}. Polarographic assays were run at least in triplicate on mitochondrial preparations obtained from distinct animals.

2.8. mPTP evaluation

Immediately after the preparation of swine heart mitochondrial fractions, fresh mitochondrial suspensions (1mg/mL) were energized in the assay buffer (130 mM KCl, 1 mM KH_2PO_4, 20 mM HEPES, pH 7.2 with TRIS), incubated at 37°C with 1 µg/mL rotenone and 5 mM succinate. To evaluate triazole effect, selected **3a** or **3b** doses were added to the mitochondrial suspensions before mPTP evaluation. mPTP opening was induced by the addition of low concentrations of Ca^{2+} (10 µM) as $CaCl_2$ solution at fixed time intervals (1 min). The calcium retention capacity (CRC), whose lowering indicates mPTP opening, was spectrofluorophotometrically evaluated in the presence of 0.8 µM Fura-FF. The probe has different spectral properties in the absence and in the presence of Ca^{2+}, namely it displays excitation/emission spectra of 365/514 nm in the absence of Ca^{2+} (Fura-FF low Ca^{2+}) and shifts to 339/507 nm in the presence of high Ca^{2+} concentrations (Fura-FF high Ca^{2+}). mPTP opening, was evaluated by the increase in the fluorescence intensity ratio (Fura-FF high Ca^{2+})/(Fura-FF low Ca^{2+}) which indicates a decrease in CRC. All measurements were processed by LabSolutions RF software. [41]

2.9. Statistical analysis

The data represent the mean ± SD (shown as vertical bars in the figures) of the number of experiments reported in the figure captions and table legends. In each set of biochemical experiments, the analyses were carried out on at least three distinct mitochondrial preparations. The differences between the enzyme activity data in differently treated mitochondria were evaluated by one way ANOVA followed by Dunnett's test when *F* values indicated significance ($P \leq 0.05$).

3. Results and discussion

3.1. Synthesis of triazole compounds

1,2,3-Triazole derivatives have good stability and high aqueous solubility in biological systems. In addition, they have structural similarity (*i.e.* planarity, size, hydrogen bond properties and dipole moment) with amide bond of enzymes, [42] which make them isosteres with the *s-trans* and *s-cis* rotamers in the conformational equilibrium of the peptide bond (Fig. 1).

Although various synthetic procedures to regioselectively produce 1,4- and 1,5-disubstituted triazoles are described in literature, [43–45] in this paper we chose to prepare 1,5-disubstituted-1,2,3-triazoles because of their larger dipolar moment than 1,4-disubstituted triazoles (5.06 debyes versus 4.31 debyes, respectively). Accordingly, most likely the inhibition of an enzyme may be affected by dipole-dipole interactions and strong hydrogen bonds with the employed substrate (Fig. 2).

More specifically, these compounds can act as hydrogen bond acceptors by exploiting the N2 and N3 nitrogen atoms of the aromatic ring and also as hydrogen bond donors *via* a CH bond. Moreover, the triazole aromatic core may be responsible for π-stacking interactions with aromatic side chains of amino acids in the active site of the enzyme target. These interactions may also be amplified by the presence of aromatic substituents on the triazole backbone.

For this reason, on considering our overt experience on the synthesis of heterocycles by 1,3-dipolar cycloaddition reaction and on the chemical interactions involved in substrates/enzyme processes, [46–48] we chose to synthesize two specific triazole derivatives, 1-benzyl-5-phenyl-1,2,3-triazole (**3a** and 1-benzyl-5-(2-nitrophenyl)-1,2,3-triazole **3b**, aiming at increasing the π-stacking and the dipole-dipole interactions by molecular moieties different from the triazole aromatic core. Accordingly, phenyl rings and nitro group are especially suitable for forming π-π and dipole-dipole interactions, respectively. In addition, the presence of the methylene group of N1-benzyl increases the degrees of freedom, allowing several interactions with the enzyme substrate.

In detail, the synthesis of 1,5-disubstituted triazoles **3a** and **3b** consists of an eliminative azide-olefin 1,3-dipolar cycloaddition (EAOC) between nitroolefins **1a-1b** as electron-deficient dipolarophile and benzylazide **2** as dipole in presence of ionic liquid 1-methyl pyridinium trifluoromethanesulfonate ([mpy]OTf) as solvent and $FeCl_3$ as Lewis acid catalyst (Scheme 1). [45]

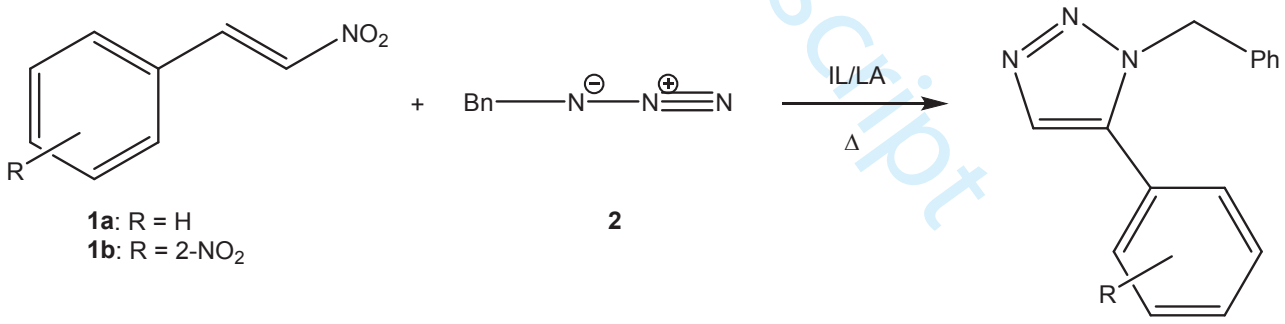

1a: R = H
1b: R = 2-NO_2

2

3a: R = H
3b: R = 2-NO_2

Scheme 1. Pattern of r 1,5-disubstituted- 1,2,3-triazole **3a** and **3b** synthesis

In detail, we selected the reusable [mpy]OTf/$FeCl_3$ system because the strong coordination of the NO_2 group to the Fe-catalyst has a large impact to the regiocontrol of the reaction, by only yielding the 1,5-regioisomer. Furthermore, the strong stabilization of reaction intermediates due to the use of the [mpy]OTf allows the formation of the instable triazoline intermediate and favours its transformation in more stable triazole compounds by eliminative mechanism. The compounds **3a** and **3b**, recovered by simple extraction in

dichloromethane and purified by flash chromatographyand obtained in 95 and 91% yield respectively, were used as model compounds for subsequent biological investigations.

3.2. 1,5-Disubstituted- 1,2,3-triazole effects on mitochondrial bioenergetics

Energy production in mitochondria in the form of ATP depends on the respiratory chain activity and ADP phosphorylation efficiency by the F_1F_O-ATPase. [49] The effects of the compounds under study on these two matched potential targets were evaluated in parallel. The effect of triazole derivatives **3a** and **3b** on mitochondrial respiration was evaluated in NADH- and succinate-energized mitochondria. Triazoles **3a** and **3b** did not significantly affect the NADH-O_2/succinate-O_2 oxidase activity (Fig. 3).

The titration curve by triazole derivatives on the Ca^{2+}- and Mg^{2+}-activated F_1F_O-ATPase(s) shows that both the compounds tested did not affect the Mg^{2+}-activated enzyme (Fig. 4B,D). Conversely, when the effect of the same compounds was tested on the Ca^{2+}-activated F_1F_O-ATPase activity, a significant enzyme inhibition was shown from 0.25 mM compound **3a** and 0.2 mM compound **3b** onwards (Fig. 4A,C). Most likely, the different effect on the two differently activated F_1F_O-ATPases depends on the enzyme conformations promoted by the cofactor(s) bound to the catalytic and/or non catalytic sites of F_1 domain. [10,12,31] The capability of different divalent cations to drive the F_1-ATPase mechanochemical coupling in mitochondria from different biological sources remains to be ascertained. However, in mammals Ca^{2+}-binding to the catalytic β subunit has been proposed as the chemical event which triggers the mPTP. [11] In the F_1 catalytic site Mg^{2+} is directly linked by βThr-163 of the P-loop and the phosphate oxygens of ATP or ADP and coordinated with three water molecules to the βArg-189, βGlu-192, βAsp-256 residues. [50] The higher Ca^{2+} radius than Mg^{2+} implies a more flexible coordination geometry characterized by irregular bond distances and angles in the β subunit catalytic sites, and the coordination geometry changes to accommodate eight ligands. [51] On these bases, the modified catalytic structure which alters the Ca^{2+}-driven catalytic mechanism of ATP hydrolysis makes the Ca^{2+}-activated F_1F_O-ATPase susceptive to triazole inhibition.

3.3. 1,5-Disubstituted- 1,2,3-triazole inhibition mechanism on the mitochondrial F_1F_O-ATPase

To understand the triazole derivatives **3a** and **3b** inhibition mechanism on the Ca^{2+}-activated F_1F_O-ATPase, further information can be obtained by kinetic studies which can lead to define the features of the enzyme–inhibitor complex in the presence or in the absence of the ATP substrate. As far as we are aware, up to now no study has considered triazole derivative effects on the F_1F_O-ATPase activity independently of potential perturbations of IMM potential and structure. Therefore, namely to detect triazole effects on these enzyme activities, uncoupled mitochondria obtained by freeze-thawing were used for kinetic analysis. Both the 1,5-disubstituted- 1,2,3-triazole (**3a** and **3b**) tested exert an uncompetitive inhibition (Fig. 5) by binding to the enzyme-ATP complex and forming the tertiary complex *ESI* (enzyme-substrate-inhibitor). This inhibition type cannot be overcome by increasing ATP concentration. Thus, both compounds do not affect the ATP binding site, but they may interfere with a binding region which modifies the Ca^{2+}-dependent catalytic mechanism of ATP hydrolysis. Moreover, the Cornish-Bowden (Fig. 5B,D) plots show that the dissociation constant of the *ESI* complex (K'_i) of the Ca^{2+}-activated F_1F_O-ATPase is 1.09±0.04 mM for compound **3a** and 1.07±0.05 mM for compound **3b** (Table 1). These similar values indicate that the *ESI* complex formation is independent of the triazole structure. However, since the inactivation rate constant is $1.93\times10^{-3}\pm0.26\times10^{-3}$ s^{-1} for **3a** and $0.86\times10^{-3}\pm0.14\times10^{-3}$ s^{-1} for **3b** (Fig. 6A), the former inhibitor shows a higher propensity to react than the latter, which implies a more rapid bond with the enzyme. The potency of a mechanism-based inhibitor, taken as k_{inact}/K'_i ratio, is a measure of the inhibitor efficiency on the Ca^{2+}-activated F_1F_O-ATPase. Since triazole derivative **3a** shows a k_{inact}/K'_i ratio 2.2 order of magnitude higher than triazole derivative **3b** (Table 1), the former inhibitor is much more powerful than the latter. Consistently, even if the two compounds show the same propensity

to form the ternary complex as reported by K'_I values, **3a** reacts with the enzyme more quickly, resulting in a more efficient Ca^{2+}-activated F_1F_O-ATPase inhibition, probably because the two compounds establish different interactions with the enzyme even if they bind on the same site on the F_1F_O-ATPase. Indeed, the inhibition by binary mixtures of triazole derivatives **3a** and **3b,** tested by the diagnostic plot for the mutual exclusion, suggests that the F_1F_O-ATPase can combine with either **3a** or **3b**, but non with both compounds (Fig. 6B). The different chemical structure of triazole derivatives resides in a nitro group in compound **3b,** which apparently does not affect the affinity for the F_1F_O-ATPase, but may require some more time to establish interactions with the enzyme.

*3.4. mPTP sensitivity to **3a** and **3b** triazole derivatives*

Recent advances strongly indicate that the Ca^{2+}-activated F_1F_O-ATPase is the lethal functional mode of the mitochondrial enzyme that triggers the mPTP. [12] The formation of this non-selective channel in functional and intact mitochondria, that normally accumulate Ca^{2+} when Ca^{2+} is stepwise provided, can be evaluated as calcium retention capacity (CRC), which decreases when the mPTP opens. According to the fluorimetric method employed, the Ca^{2+} release from mitochondria ascribed to mPTP opening is revealed by an increase in the fluorescence intensity ratio (Fura-FF high Ca^{2+})/(Fura-FF low Ca^{2+}). Consistently with the selective F_1F_O-ATPase inhibition by compounds **3a** and **3b** when the natural cofactor Mg^{2+} is replaced by Ca^{2+} (Fig. 4), the mPTP formation in triazole-treated mitochondria is inhibited (Fig. 7). Accordingly, the increase in CRC upon subsequent 10 µM Ca^{2+} additions at fixed time intervals, shown by the rise in the (Fura-FF high Ca^{2+})/(Fura-FF low Ca^{2+}) ratio, indicates that in presence of the compounds tested, mitochondria attain a higher threshold value of Ca^{2+} concentration to trigger mPTP formation (Fig. 7A); in other words more Ca^{2+} additions are required to promote mPTP opening (Fig. 7B). Noteworthy, the two compounds behave differently as mPTP inhibitors. Accordingly, triazole **3a** attains a lower CRC value (high Fura-FF ratio) than triazole **3b** when mPTP opens. We can speculate that the different effects on mPTP of the two compounds under study are due to the onset of different kinds of interactions on the Ca^{2+}-activated F_1F_O-ATPase which affect the mPTP size [52] even if their have the same binding region (Fig. 6B). On these bases, a lower CRC value would mirror a larger mPTP size. Moreover, the sharp increase in fluorescence followed by a less sharp decline as mitochondria take up calcium in presence of triazole **3a** has a gradual increase of baseline with each Ca^{2+} pulse. We could assert that the trend could be due to an inhibitory effect of the mitochondrial calcium uniporter uptake. [53]

4. Conclusions

The link between the inhibition power of the bioactive triazoles and their chemical structure could draw the road to address further developments in pharmacology, which can be helpful in medical chemistry to fight mPTP-related human pathologies. Consistently, the F_1F_O-ATPase as main candidate component of mPTP should be a mitochondrial target of these compounds to lessen or block the mPTP formation. Since the different selectivity and interaction rate of structurally different compounds on the Ca^{2+}-activated F_1F_O-ATPase is not directly related to their mPTP inhibition efficiency, most likely the 1,5-disubstituted- 1,2,3-triazoles tested mainly act on the subunits of F_1F_O-ATPase(s) involved in the mechanism of mPTP formation. On balance, the slowdown of mPTP formation (desensitization) could be indirectly due to changes in the conformational transmission mechanism from F_1 to F_O that opens the mPTP.

Acknowledgements

Danilo Matteuzzi (Department of Veterinary Medical Sciences, University of Bologna) is gratefully acknowledged for kindly conferring swine hearts from a local abattoir to Biochemistry laboratories.

This work was financed by a RFO grant from the University of Bologna, from Carisbo Foundation (Grant n° 2018/0375), Bologna, Italy and by a research grant from Calabria Region (PAC CALABRIA 2014-2020 - Asse Prioritario 12, Azione B) 10.5.12 CUP: H28D19000040006) and the University of Calabria.

References

1. Zoratti M. & I. Szabò. 1995. The mitochondrial permeability transition. *Biochim. Biophys. Acta* **1241**: 139–176.
2. Bernardi P., A. Rasola, M. Forte, *et al.* 2015. The Mitochondrial Permeability Transition Pore: Channel Formation by F-ATP Synthase, Integration in Signal Transduction, and Role in Pathophysiology. *Physiol. Rev.* **95**: 1111–1155.
3. Briston T., D.L. Selwood, G. Szabadkai, *et al.* 2019. Mitochondrial Permeability Transition: A Molecular Lesion with Multiple Drug Targets. *Trends Pharmacol. Sci.* **40**: 50–70.
4. Urbani A., V. Giorgio, A. Carrer, *et al.* 2019. Purified F-ATP synthase forms a Ca2+-dependent high-conductance channel matching the mitochondrial permeability transition pore. *Nat Commun* **10**: 4341.
5. Mnatsakanyan N., M.C. Llaguno, Y. Yang, *et al.* 2019. A mitochondrial megachannel resides in monomeric F1FO ATP synthase. *Nat Commun* **10**: 5823.
6. Kühlbrandt W. 2019. Structure and Mechanisms of F-Type ATP Synthases. *Annu. Rev. Biochem.* **88**: 515–549.
7. Nesci S., F. Trombetti, V. Ventrella, *et al.* 2015. Opposite rotation directions in the synthesis and hydrolysis of ATP by the ATP synthase: hints from a subunit asymmetry. *J. Membr. Biol.* **248**: 163–169.
8. Junge W., H. Sielaff & S. Engelbrecht. 2009. Torque generation and elastic power transmission in the rotary F(O)F(1)-ATPase. *Nature* **459**: 364–370.
9. Frasch W.D. 2000. The participation of metals in the mechanism of the F(1)-ATPase. *Biochim. Biophys. Acta* **1458**: 310–325.
10. Nesci S., F. Trombetti, V. Ventrella, *et al.* 2017. Kinetic properties of the mitochondrial F1FO-ATPase activity elicited by Ca(2+) in replacement of Mg(2+). *Biochimie* **140**: 73–81.
11. Giorgio V., V. Burchell, M. Schiavone, *et al.* 2017. Ca(2+) binding to F-ATP synthase β subunit triggers the mitochondrial permeability transition. *EMBO Rep.* **18**: 1065–1076.
12. Algieri C., F. Trombetti, A. Pagliarani, *et al.* 2019. Mitochondrial Ca2+ -activated F1 FO -ATPase hydrolyzes ATP and promotes the permeability transition pore. *Ann. N. Y. Acad. Sci.* **1457**: 142–157.
13. Nesci S. 2020. The mitochondrial permeability transition pore in cell death: A promising drug binding bioarchitecture. *Medicinal Research Reviews* **40**: 811–817.
14. Baines C.P., R.A. Kaiser, N.H. Purcell, *et al.* 2005. Loss of cyclophilin D reveals a critical role for mitochondrial permeability transition in cell death. *Nature* **434**: 658–662.
15. Nesci S. 2020. The mitochondrial permeability transition pore in cell death: A promising drug binding bioarchitecture. *Medicinal Research Reviews* **40**:.
16. Thirumurugan P., D. Matosiuk & K. Jozwiak. 2013. Click chemistry for drug development and diverse chemical-biology applications. *Chem. Rev.* **113**: 4905–4979.
17. Angell Y.L. & K. Burgess. 2007. Peptidomimetics via copper-catalyzed azide-alkyne cycloadditions. *Chemical Society Reviews* **36**: 1674–1689.
18. Singhal N., P.K. Sharma, R. Dudhe, *et al.* 2011. Recent advancement of triazole derivatives and their biological significance. *Journal of Chemical and Pharmaceutical Research* **3**: 126–133.
19. Huisgen R. 1963. 1,3-Dipolar Cycloadditions. Past and Future. *Angewandte Chemie International Edition in English* **2**: 565–598.

20. Tornøe C.W., C. Christensen & M. Meldal. 2002. Peptidotriazoles on solid phase: [1,2,3]-triazoles by regiospecific copper(i)-catalyzed 1,3-dipolar cycloadditions of terminal alkynes to azides. *J. Org. Chem.* **67**: 3057–3064.
21. Boren B.C., S. Narayan, L.K. Rasmussen, *et al.* 2008. Ruthenium-catalyzed azide-alkyne cycloaddition: scope and mechanism. *J. Am. Chem. Soc.* **130**: 8923–8930.
22. Huisgen R., G. Szeimies & L. Möbius. 1966. 1.3-Dipolare Cycloadditionen, XXIV. Triazoline aus organischen Aziden und α.β-ungesättigten Carbonylverbindungen oder Nitrilen. *Chemische Berichte* **99**: 475–490.
23. Broeckx W., N. Overbergh, C. Samyn, *et al.* 1971. Cycloaddition reactions of azides with electron-poor olefins: Isomerization and thermolysis of the resulting Δ2-triazolines. *Tetrahedron* **27**: 3527–3534.
24. Wang Y.-C., Y.-Y. Xie, H.-E. Qu, *et al.* 2014. Ce(OTf)3-Catalyzed [3 + 2] Cycloaddition of Azides with Nitroolefins: Regioselective Synthesis of 1,5-Disubstituted 1,2,3-Triazoles. *J. Org. Chem.* **79**: 4463–4469.
25. Maiuolo L., B. Russo, V. Algieri, *et al.* 2019. Regioselective synthesis of 1,5-disubstituted 1,2,3-triazoles by 1,3-dipolar cycloaddition: Role of Er(OTf)3, ionic liquid and water. *Tetrahedron Letters* **60**: 672–674.
26. Nino A.D., V. Algieri, M.A. Tallarida, *et al.* 2019. Regioselective Synthesis of 1,4,5-Trisubstituted-1,2,3-Triazoles from Aryl Azides and Enaminones. *European Journal of Organic Chemistry* **2019**: 5725–5731.
27. Šileikytė J., J. Devereaux, J. de Jong, *et al.* 2019. Second-Generation Inhibitors of the Mitochondrial Permeability Transition Pore with Improved Plasma Stability. *ChemMedChem* **14**: 1771–1782.
28. Bortolini O., A.D. Nino, A. Garofalo, *et al.* 2010. Mild oxidative conversion of nitroalkanes into carbonyl compounds in ionic liquids. *Synthetic Communications* **40**: 2483–2487.
29. De Nino A., L. Maiuolo, P. Merino, *et al.* 2015. Efficient organocatalyst supported on a simple ionic liquid as a recoverable system for the asymmetric diels-alder reaction in the presence of water. *ChemCatChem* **7**: 830–835.
30. Bortolini O., A. De Nino, A. Garofalo, *et al.* 2010. Erbium triflate in ionic liquids: A recyclable system of improving selectivity in Diels-Alder reactions. *Applied Catalysis A: General* **372**: 124–129.
31. Nesci S., V. Ventrella, F. Trombetti, *et al.* 2016. Preferential nitrite inhibition of the mitochondrial F1FO-ATPase activities when activated by Ca(2+) in replacement of the natural cofactor Mg(2+). *Biochim. Biophys. Acta* **1860**: 345–353.
32. Bradford M.M. 1976. A rapid and sensitive method for the quantitation of microgram quantities of protein utilizing the principle of protein-dye binding. *Anal. Biochem.* **72**: 248–254.
33. Nesci S., V. Ventrella, F. Trombetti, *et al.* 2014. The mitochondrial F1FO-ATPase desensitization to oligomycin by tributyltin is due to thiol oxidation. *Biochimie* **97**: 128–137.
34. Nesci S., V. Ventrella, F. Trombetti, *et al.* 2014. Thiol oxidation is crucial in the desensitization of the mitochondrial F1FO-ATPase to oligomycin and other macrolide antibiotics. *Biochim. Biophys. Acta* **1840**: 1882–1891.
35. Nesci S., F. Trombetti, M. Pirini, *et al.* 2016. Mercury and protein thiols: Stimulation of mitochondrial F1FO-ATPase and inhibition of respiration. *Chem. Biol. Interact.* **260**: 42–49.
36. Cornish-Bowden A. 1974. A simple graphical method for determining the inhibition constants of mixed, uncompetitive and non-competitive inhibitors. *Biochem. J.* **137**: 143–144.
37. Mizutani K., M. Yamamoto, K. Suzuki, *et al.* 2011. Structure of the rotor ring modified with N,N'-dicyclohexylcarbodiimide of the Na+-transporting vacuolar ATPase. *Proc. Natl. Acad. Sci. U.S.A.* **108**: 13474–13479.
38. Nesci S., V. Ventrella, F. Trombetti, *et al.* 2013. Mussel and mammalian ATP synthase share the same bioenergetic cost of ATP. *J. Bioenerg. Biomembr.* **45**: 289–300.
39. Yonetani T. 1982. The Yonetani-Theorell graphical method for examining overlapping subsites of enzyme active centers. *Meth. Enzymol.* **87**: 500–509.
40. Nicholls D.G. & S.J. Ferguson. 2013. 5 - Respiratory Chains. In *Bioenergetics (Fourth Edition)* Nicholls D.G. & Ferguson S.J., Eds. 91–157. Boston: Academic Press.
41. Algieri C., F. Trombetti, A. Pagliarani, *et al.* 2020. Phenylglyoxal inhibition of the mitochondrial F1FO-ATPase activated by Mg2+ or by Ca2+ provides clues on the mitochondrial permeability transition pore. *Arch. Biochem. Biophys.* **681**: 108258.
42. Miriam Corredor, J.S. Jordi Solà & Ignacio AlfonsoIgnacio Alfonso. Disubstituted 1,2,3-Triazoles as Amide Bond Mimetics. *Targets in Heterocyclic Systems* **21**: 1–22.

43. Rostovtsev V.V., L.G. Green, V.V. Fokin, *et al.* 2002. A Stepwise Huisgen Cycloaddition Process: Copper(I)-Catalyzed Regioselective "Ligation" of Azides and Terminal Alkynes. *Angewandte Chemie International Edition* **41**: 2596–2599.
44. Gangaprasad D., J. Paul Raj, T. Kiranmye, *et al.* 2016. A tunable route to oxidative and eliminative [3+2] cycloadditions of organic azides with nitroolefins: CuO nanoparticles catalyzed synthesis of 1,2,3-triazoles under solvent-free condition. *Tetrahedron Letters* **57**: 3105–3108.
45. De Nino A., P. Merino, V. Algieri, *et al.* 2018. Synthesis of 1,5-functionalized 1,2,3-triazoles using ionic liquid/iron(III) chloride as an efficient and reusable homogeneous catalyst. *Catalysts* **8**:.
46. Maiuolo L., V. Algieri, F. Olivito, *et al.* 2020. Recent Developments on 1,3-Dipolar Cycloaddition Reactions by Catalysis in Green Solvents. *Catalysts* **10**: 65–91.
47. Maiuolo L., A. De Nino, V. Algieri, *et al.* 2017. Microwave-assisted 1,3-dipolar cyclo-addition: Recent advances in synthesis of isoxazolidines. *Mini-Reviews in Organic Chemistry* **14**: 136–142.
48. Merino P., L. Maiuolo, I. Delso, *et al.* 2017. Chemical approaches to inhibitors of isoprenoid biosynthesis: targeting farnesyl and geranylgeranyl pyrophosphate synthases. *RSC Advances* **7**: 10947–10967.
49. Nicholls D. 1984. Chapter 2 Mechanisms of energy transduction. In *New Comprehensive Biochemistry* Ernster L., Ed. 29–48. Elsevier.
50. Rees D.M., M.G. Montgomery, A.G.W. Leslie, *et al.* 2012. Structural evidence of a new catalytic intermediate in the pathway of ATP hydrolysis by F1-ATPase from bovine heart mitochondria. *Proc. Natl. Acad. Sci. U.S.A.* **109**: 11139–11143.
51. Casadio R. & B.A. Melandri. 1996. CaATP inhibition of the MgATP-dependent proton pump (H+-ATPase) in bacterial photosynthetic membranes with a mechanism of alternative substrate inhibition. *Journal of Biological Inorganic Chemistry* **1**: 284–291.
52. Neginskaya M.A., M.E. Solesio, E.V. Berezhnaya, *et al.* 2019. ATP Synthase C-Subunit-Deficient Mitochondria Have a Small Cyclosporine A-Sensitive Channel, but Lack the Permeability Transition Pore. *Cell Rep* **26**: 11-17.e2.
53. Marchi S., V.A.M. Vitto, S. Patergnani, *et al.* 2019. High mitochondrial Ca2+ content increases cancer cell proliferation upon inhibition of mitochondrial permeability transition pore (mPTP). *Cell Cycle* **18**: 914–916.

Figure legends

Figure 1. Peptide conformational equilibrium s-trans/s-cis and 1,5-disubstituted triazole isosteres.

Figure 2. Summary of potential binding interactions for 1,4- and 1,5-disubstituted-1,2,3-triazoles.

Figure 3. 1,5-Disubstituted- 1,2,3-triazole effect on mitochondrial respiration. A) NADH-O_2 (green vertical bars) and Succinate-O_2 (red vertical bars) oxidase activity were evaluated without and with 1 mM of triazole derivatives **3a** and **3b**. Data expressed as column chart represent the mean ± SD from three experiments carried out on different mitochondrial preparations. B) Representative traces of the respiration recordings by NADH (up traces) and by succinate addition (down traces). The arrows indicate the addition of the substrates.

Figure 4. Effect of triazole derivatives **3a** and **3b** on activity of mitochondrial Ca^{2+} and Mg^{2+}-activated F_1F_O-ATPase. Ca^{2+}-activated F_1F_O-ATPase (○) and Mg^{2+}-activated F_1F_O-ATPase activities (●) in the presence of increasing concentrations of compound **3a** (A,B) and compound **3b** (C,D). Data represent the mean ± SD from

three independent experiments carried out on distinct mitochondrial preparations. * indicates significant differences with respect to the control without triazoles ($P \leq 0.05$).

Figure 5. Ca^{2+}-activated F_1F_O-ATPase inhibition by triazole derivatives **3a** and **3b**. Dixon (A, C) and Cornish–Bowden (B, D) plots obtained at 1 mM (○) or 3 mM (●) ATP for the Ca^{2+}-activated F_1F_O-ATPase (A,B); 3 mM (□) or 6 mM (■) ATP for the Mg^{2+}-F_1F_O-activated ATPase (C, D) and designing the experiments as detailed in Section 4.2.4. All points represent the mean ± SD (vertical bars) of four distinct experiments carried out on distinct mitochondrial preparations.

Figure 6. Kinetics of the Ca^{2+}-activated F_1F_O-ATPase inhibition by triazole derivatives **3a** and **3b**. A) Time course plot of Ca^{2+}-activated F_1F_O-ATPase to obtain the inactivation rate constant (k_{inact}) as detailed in Section 4.2.4 with 1 mM of compound **3a** (□) and 1 mM of compound **3b** (■). B) Multiple inhibitor analysis by Dixon plots for the Ca^{2+}-activated F_1F_O-ATPase inhibition by compound **3b**. The F-ATPase assay were carried out in the absence (○) or in the presence of 0.5 mM compound **3a** (●). Each point represents the mean value ± SD (vertical bars) of at least three experiments carried out on distinct mitochondrial preparations.

Figure 7. Evaluation of mPTP opening. Representative curves (A) of the calcium retention capacity (CRC) expressed as Fura-FF ratio (Fura-FF high Ca^{2+})/(Fura-FF low Ca^{2+}), evaluated in response to subsequent 10 µM $CaCl_2$ pulses (shown by the triangles), as detailed in Section 4.2.6, in untreated mitochondria (Control), and in the presence of 2 mM MgADP, 1.0 mM compound **3a**, 1.0 mM compound **3b**. B) Quantitation of the mPTP is expressed as the ratio of the number of calcium pulses required to induce the mPTP in MgADP inhibited (CRC_i) and untreated (CRC_o) mitochondria. Data represent the mean ± SD from three independent experiments carried out on distinct mitochondrial preparations. * indicates significant differences with respect to the control ($P \leq 0.05$).

Table 1. Inhibition kinetic parameters of the Ca^{2+}-activated F_1F_O-ATPase activity by triazole compounds

	Compound **3a**	Compound **3b**
K'_i (mM)	1.09±0.04	1.07±0.05
k_{inact} (s^{-1})	$1.93x10^{-3}$±$0.26x10^{-3}$	$0.86x10^{-3}$±$0.14x10^{-3}$
k_{inact}/K'_i ($mM^{-1}·s^{-1}$)	$1.77x10^{-3}$	$0.80x10^{-3}$

The K'_i values (dissociation constant of the *ESI* complex) were graphically obtained from the Cornish plots drawn in Fig. 5B,D as detailed in Section 2.6. The k_{inact} values (inactivation rate constant) were graphically obtained from the plots in Fig. 6A as detailed in the section 2.6. Data are the mean values obtained from three sets of experiments carried out on distinct mitochondrial preparations.

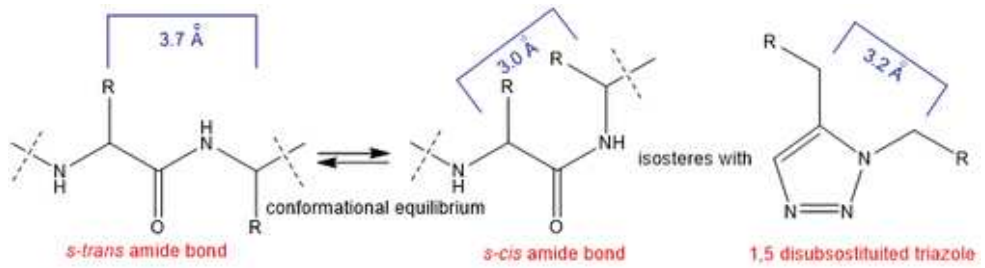

Figure 1. Peptide conformational equilibrium s-trans/s-cis and 1,5-disubstituted triazole isosteres.

21x5mm (600 x 600 DPI)

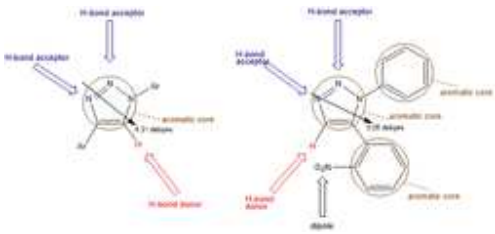

Figure 2. Summary of potential binding interactions for 1,4- and 1,5-disubstituted-1,2,3-triazoles.

10x4mm (600 x 600 DPI)

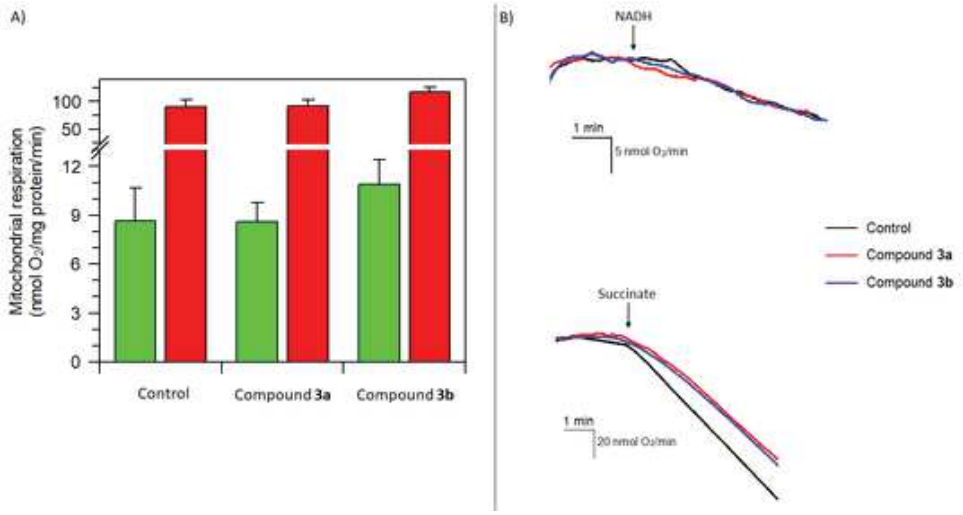

Figure 3. 1,5-Disubstituted- 1,2,3-triazole effect on mitochondrial respiration. A) NADH-O2 (green vertical bars) and Succinate-O2 (red vertical bars) oxidase activity were evaluated without and with 1 mM of triazole derivatives 3a and 3b. Data expressed as column chart represent the mean ± SD from three experiments carried out on different mitochondrial preparations. B) Representative traces of the respiration recordings by NADH (up traces) and by succinate addition (down traces). The arrows indicate the addition of the respective substrate.

22x12mm (600 x 600 DPI)

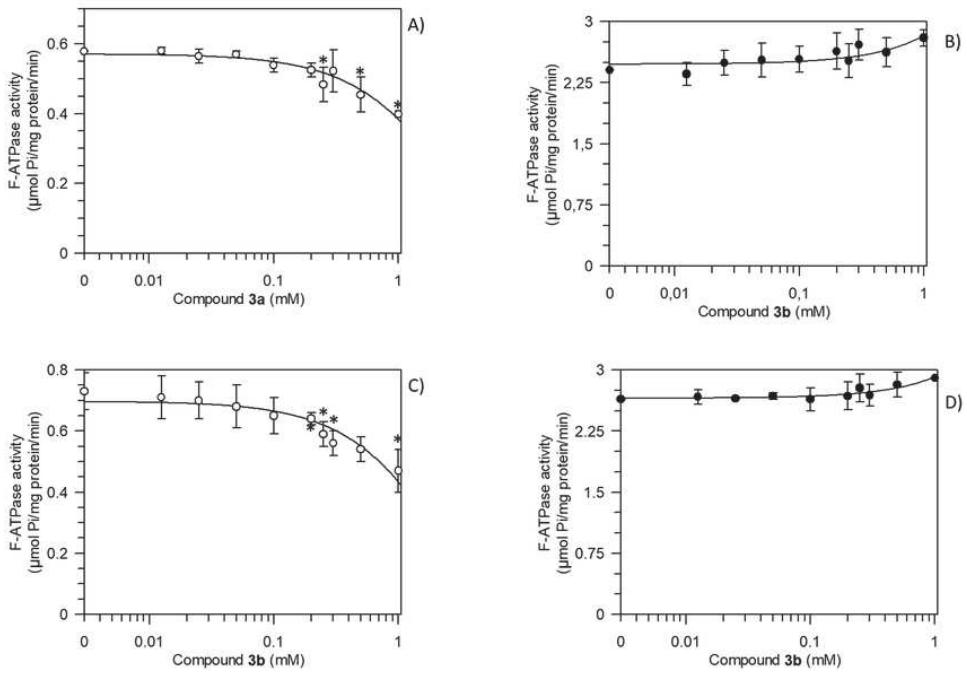

Figure 4. Effect of triazole derivatives 3a and 3b on activity of mitochondrial Ca2+ and Mg2+-activated F1FO-ATPase. Ca2+-activated F1FO-ATPase (○) and Mg2+-activated F1FO-ATPase activities (●) in the presence of increasing concentrations of compound 3a (A,B) and compound 3b (C,D). Data represent the mean ± SD from three independent experiments carried out on distinct mitochondrial preparations. * indicates significant differences with respect to the control without triazoles (P≤0.05).

36x25mm (600 x 600 DPI)

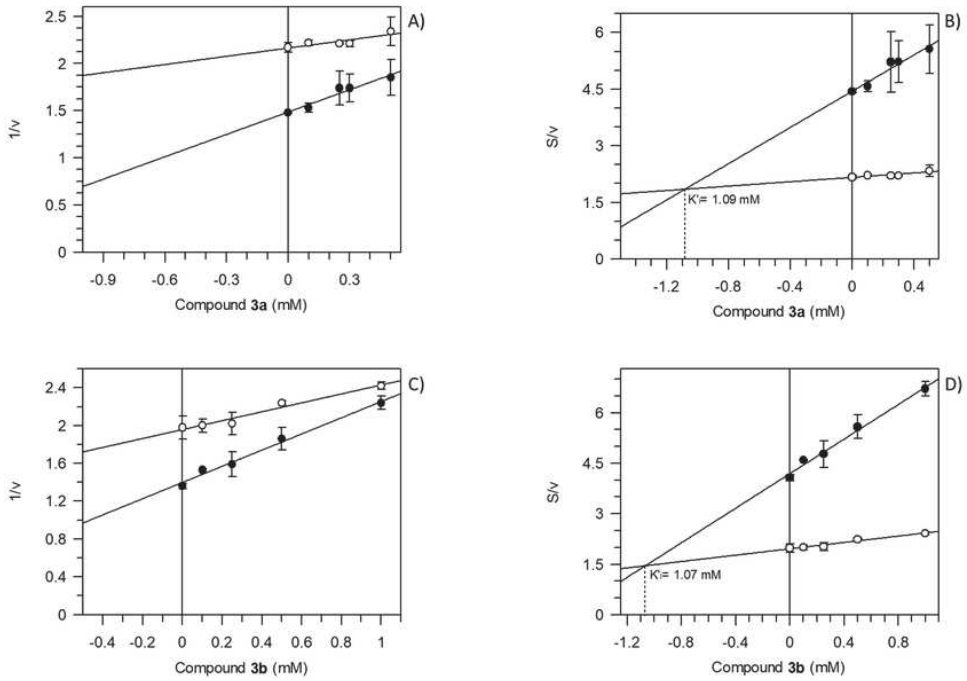

Figure 5. Ca2+-activated F1FO-ATPase inhibition by triazole derivatives 3a and 3b. Dixon (A, C) and Cornish–Bowden (B, D) plots obtained at 1 mM (○) or 3 mM (●) ATP for the Ca2+-activated F1FO-ATPase (A,B); 3 mM (□) or 6 mM (■) ATP for the Mg2+-F1FO-activated ATPase (C, D) and designing the experiments as detailed in Section 4.2.4. All points represent the mean ± SD (vertical bars) of four distinct experiments carried out on distinct mitochondrial preparations.

35x25mm (600 x 600 DPI)

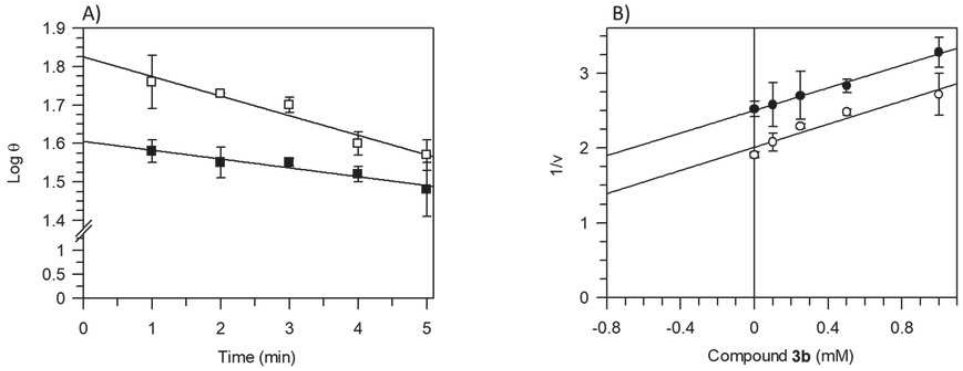

Figure 6. Kinetics of the Ca2+-activated F1FO-ATPase inhibition by triazole derivatives 3a and 3b. A) Time course plot of Ca2+-activated F1FO-ATPase to obtain the inactivation rate constant (kinact) as detailed in Section 4.2.4 with 1 mM of compound 3a (□) and 1 mM of compound 3b (■). B) Multiple inhibitor analysis by Dixon plots for the Ca2+-activated F1FO-ATPase inhibition by compound 3b. The F-ATPase assay were carried out in the absence (○) or in the presence of 0.5 mM compound 3a (●). Each point represents the mean value ± SD (vertical bars) of at least three experiments carried out on distinct mitochondrial preparations.

37x14mm (600 x 600 DPI)

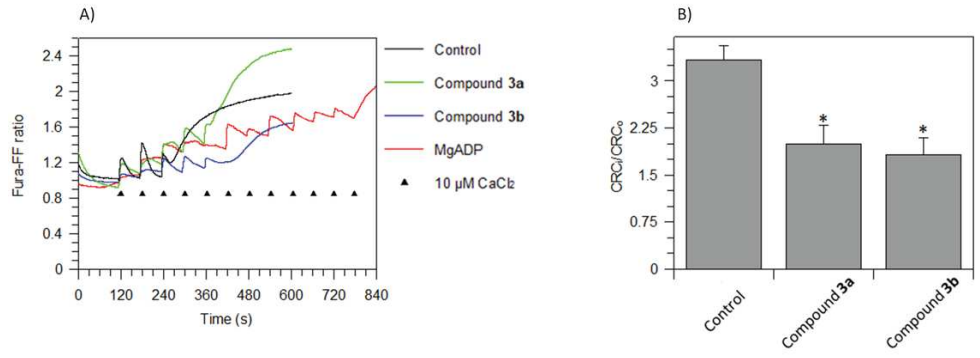

Figure 7. Evaluation of mPTP opening. Representative curves (A) of the calcium retention capacity (CRC) expressed as Fura-FF ratio (Fura-FF high Ca2+)/(Fura-FF low Ca2+), evaluated in response to subsequent 10 µM CaCl2 pulses (shown by the triangles), as detailed in Section 4.2.6, in untreated mitochondria (Control), and in the presence of 2 mM MgADP, 1.0 mM compound 3a, 1.0 mM compound 3b. B) Quantitation of the mPTP is expressed as the ratio of the number of calcium pulses required to induce the mPTP in MgADP inhibited (CRCi) and untreated (CRCo) mitochondria. Data represent the mean ± SD from three independent experiments carried out on distinct mitochondrial preparations. * indicates significant differences with respect to the control (P≤0.05).

48x18mm (600 x 600 DPI)